Heat Transfer and Flow Characteristics of an Oblique Turbulent Impinging Jet Within Confined Walls

K. Ichimiya
Department of Mechanical System Engineering,
Yamanashi University,
Takeda-4, Kofu,
Yamanashi, 400 Japan

Experiments were conducted to determine the turbulent heat transfer and flow characteristics of an oblique impinging circular jet within closely confined walls using air as a working fluid. The local temperature distribution on the impingement surface was obtained in detail by a thermocamera using a liquid crystal sheet. A correction to the heat flux was evaluated by using the detailed temperature distribution and solving numerically the three-dimensional equation of heat conduction in the heated section. Two-dimensional profiles of the local Nusselt numbers and temperatures changed with jet angle and Reynolds number. These showed a peak shift toward the minor flow region and a plateau of the local heat transfer coefficients in the major flow region. The local velocity and turbulent intensity in the gap between the confined insulated wall and impingement surface were also obtained in detail by a thermal anemometer.

Introduction

Impinging jets are used to improve the local heat transfer in various applications, including gas turbine cooling (Han et al., 1983), temperature equalization for a slab in continuous casting direct rolling process (Ichimiya et al., 1987), and cooling of electronics (Hollworth and Durbin, 1992). Martin (1977), Jambunathan et al. (1992), and Viskanta (1993) provided a comprehensive list of the available literature on impingement cooling. In practical applications, the orientation of the nozzle in relatively narrow spaces with confined walls is an important factor, together with the compactness of the facility. McMurray et al. (1966) experimented with an impinging jet flow for removing heat from a hot plate and, in so doing, configured the local heat transfer on the impingement surface by control of inclination angle. Sparrow and Lovell (1980) examined the shift of the position of maximum heat transfer coefficient for various inclination angles by using similarity between mass transfer and heat transfer. Goldstein and Franchett (1988) conducted experiments to determine the heat transfer to a jet impinging at different angles on a flat surface using a surface heater and liquid crystal. Contours of constant temperature (color: red) in the liquid crystal were obtained at different heat fluxes. The local Nusselt number was correlated by an exponential relationship, which included the local position and jet orientation. Stevens and Webb (1991) obtained an empirical equation for local heat transfer coefficient that includes the inclination angle. This research was performed on an impinging jet without confining walls. Ward et al. (1991) determined the local heat transfer associated with impinging air jets within a confined crossflow by using the mass transfer analogy technique.

With an oblique impinging jet, Foss and Kleis (1976) reported the mean flow characteristics, surface isobars, streamwise vorticity, and stagnation point location, for jet inclination angles less than 12 deg. Kamoi and Tanaka (1977) measured the static pressure distribution, velocity distribution, and shear stresses with various levels of turbulence at nozzle exit for inclination angles ranging from 30 to 90 deg. Foss (1979) measured the turbulence intensity values near the impingement surface, isopressure distribution on the surface and velocity vectors distribution for an inclination angle of 45 deg. Rubel (1981, 1982) analyzed the flow at the jet impingement zone. These previous studies were performed in a system without confined walls.

In the present paper, the impinging flow and turbulent heat transfer characteristics of an inclined circular jet within a channel with confining walls of comparatively narrow space ($h/D = 1.0$) are examined experimentally. The surface temperature was measured by the liquid crystal technique as recorded by an image processor. With this technique, isothermal lines on the impingement surface were determined without a large number of thermocouples or without changing heat flux level. In addition, the velocity distribution, the turbulence intensity, and the power spectrum of velocity fluctuation were examined experimentally for each case and correlations are made with heat transfer results.

Experimental Apparatus and Procedure

A schematic diagram of the experimental apparatus is shown in Fig. 1. The apparatus is composed of the flow delivery passage, the heated section including the surface upon which the flow impinges, and the measuring system. After the air impinges upon the heated surface from an inclined circular nozzle of 30 mm diameter, it is released to the atmosphere. The distance between the nozzle and the impingement surface is 30 mm. The upper wall, set at the same level the nozzle, is made of acrylic resin and is thermally insulated. The inclined angles, θ (refer to Fig. 2), are 45, 60, and 90 deg from horizontal. The shape of the nozzle exit is a circle in the case of $\theta = 90$ deg and an ellipse in the other cases. The impingement section is composed of an transparent acrylic plate, a thermosensitive liquid crystal sheet, and a stainless steel foil 20 μm thick. These were closely connected by binding tapes with transparency 99 percent. The foil was heated electrically. The impingement surface temperature was measured by transforming the color intensity of the liquid crystal sheet to the corresponding temperature (refer to the section "Temperature Measurement"). The back side of the impingement section was illuminated by four 100-W tungsten halogen lamps. Illumination was from a low angle so that light was not specularly reflected to the CCD (Charge-Coupled Device) camera. These lamps were equipped with infrared radiation absorbing filters to prevent radiative heating of the liquid crystal. Three kinds of optical filters were mounted, one after another, in

Contributed by the Heat Transfer Division and presented at the 29th National Heat Transfer Conference, Atlanta, Georgia, August 8–11, 1993. Manuscript received by the Heat Transfer Division October 1993; revision received April 1994. Keywords: Augmentation and Enhancement, Forced Convection, Measurement Techniques. Associate Technical Editor: T. Simon.

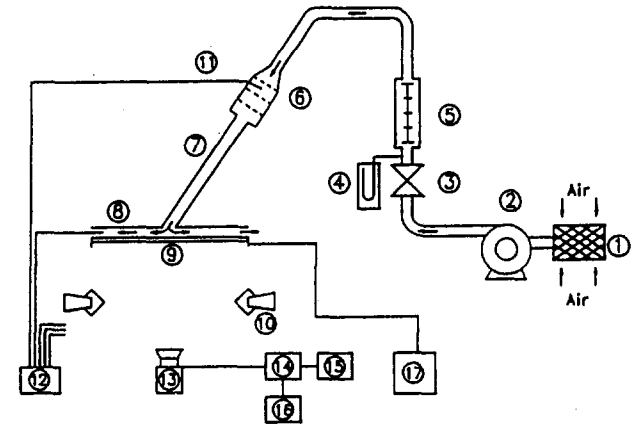

Fig. 1 Schematic diagram of experimental facility

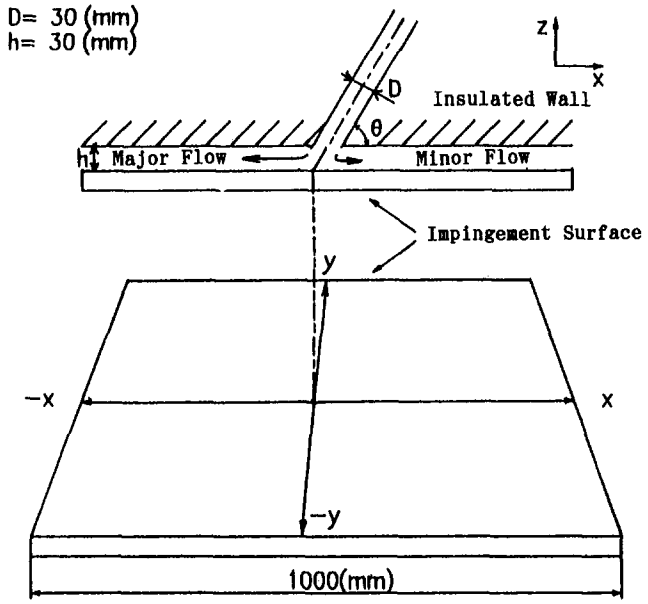

Fig. 2 Coordinate system

front of the camera lens. The color image was converted into an electrical signal by a CCD camera. The measuring region was divided into 128 × 128 pixels (the size of one pixel is 1 mm × 1.25 mm).

The local heat transfer coefficient, α, and the local Nusselt number, Nu, on the impingement surface were calculated by the following equations, which use the net heat flux q_{net} (refer to the section "Correction of Local Heat Flux") and the mixed mean temperature at the nozzle exit, T_{in},

$$\alpha = q_{net}/(T_w - T_{in}) \tag{1}$$

$$\mathrm{Nu} = \alpha \cdot D/\lambda \tag{2}$$

where λ is the thermal conductivity of the fluid.

Velocity and turbulence intensity across the section were measured in unheated condition by a thermal anemometer (single wire probe) to document the flow at Re = 2×10^4 (u_0 = 11 m/s). A probe was set to face the flow and be parallel to the impingement surface. The jet flow was classified into the major flow along the negative side of X and the minor flow along the positive side of X (refer to Fig. 2). Experimental conditions are as follows: The diameter of the nozzle is D = 30 mm; the distance between the nozzle and the impingement surface, h, is 30 mm; the Reynolds numbers based upon the nozzle diameter, Re, are 2×10^4, 10^4, 5000, and 2000; and the angles of inclination, θ, are 90, 60, and 45 deg. The flow at nozzle exit was nearly fully developed and the exit turbulence intensity ranged from 2 to 6 percent for Re = 2×10^4. The temperature difference between the impingement surface and the fluid ranged from 10°C to 15°C.

Temperature Measurement

The liquid crystal was a mixture of cholesteric nonanoate and cholesteric chloride. It was microencapsulized and bound between a transparent plate and a stainless steel foil. The relationship between light brightness from the liquid crystal and temperature was calibrated in advance (Akino et al., 1989). Calibration tests were carried out changing temperature gradients to determine accuracy and resolution. The scattered reflected light from the liquid crystal at a given temperature, T, was divided into three main color components—red, green, and blue—by optical filters, and the brightness of each component was obtained at each pixel as the image data. The temperature, T, was estimated by the regression equation including the relative brightness (r, g, b),

$$T = \xi \cdot r + \eta \cdot g + \gamma \cdot b + \delta \tag{3}$$

The values of r, g, and b were defined as follows:

$$r = R/S, \quad g = G/S, \quad b = B/S$$

where R, G, and B were the brightness values and S was the total $S = R + G + B$. The regression coefficients ξ, η, γ, and δ were

Nomenclature

B = brightness value
D = nozzle diameter
G_{aa} = power spectrum
G = brightness value
h = distance between nozzle and impingement surface
H = dimensionless distance between nozzle and impingement surface = h/D
Nu = Nusselt number = $\alpha \cdot D/\lambda$
q_{acr} = corrected heat flux in acrylic plate
q_{cond} = corrected heat flux in the heated section = $q_{acr} + q_{sus}$
q_{net} = net heat flux
q_{rad} = radiative heat flux
q_{sus} = corrected heat flux in stainless steel foil
q_{unif} = uniform heat flux by Joule heating
R = brightness value
Re = Reynolds number = $u_0 \cdot D/\nu$
S = total brightness = $R + G + B$
T = temperature
T_{in} = fluid temperature at nozzle exit
T_w = impingement surface temperature
u = velocity
u_{max} = maximum velocity at nozzle exit
u_0 = average velocity at nozzle exit
x = x coordinate (refer to Fig. 2)
X = dimensionless x coordinate = x/D
y = y coordinate (refer to Fig. 2)
Y = dimensionless y coordinate = y/D
z = z coordinate (refer to Fig. 2)
Z = dimensionless z coordinate = z/D
α = local heat transfer coefficient = $q_{net}/(T_w - T_{in})$
θ = inclination angle of nozzle
λ = thermal conductivity of fluid
ν = kinetic viscosity of fluid

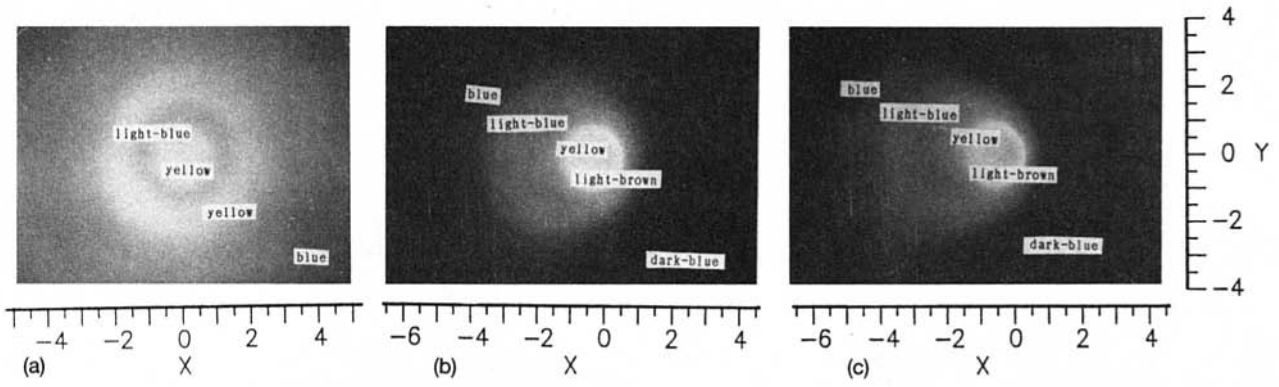

Fig. 3 Color-temperature visualization (Re = 2 × 10⁴): (a) θ = 90 deg, (b) θ = 60 deg, (c) θ = 45 deg

determined using the groups of the temperature and brightness data for optical filters. In the present experiment, these constant values were $\xi = 2.29678$, $\eta = 5.78914$, $\gamma = 19.9525$, and $\delta = 30.4762$ and have the unit of temperature °C. The temperatures were measured in the range of 35 ~ 42°C and the accuracy was within 0.2°C. The colors were brown, orange, yellow, green, and blue ranging from low temperature to high temperature.

Correction of Local Heat Flux

The local heat flux must be corrected locally using the detailed temperature distribution (Kunugi et al., 1991). The heat flow in the acrylic plate and the stainless steel foil was estimated as a steady thermal conduction problem. Thermal conduction without heat generation is expressed by the following equation:

$$\nabla^2 T = 0 \tag{4}$$

In the acrylic plate, the three-dimensional thermal conduction equation was solved numerically at all pixels. The temperature distribution on one side was given by the measured values and another five sides were insulated thermally. The distribution of heat flux q_{acr} was estimated from the calculated temperature in the plate. In the stainless steel foil, the heat flux q_{sus} was calculated in a two-dimensional system because the foil was thinner than the size of one pixel. Additionally, the radiation loss from the impingement surface was evaluated. Consequently, the net heat flux q_{net} from the impingement surface to the fluid was obtained as the following equation:

$$q_{net} = q_{unif} + q_{aor} + q_{sus} - q_{rad} \tag{5}$$

where q_{unif} is the uniform heat flux by Joule heating (power supply over unit surface to the stainless steel foil), q_{aor} the corrected heat flux in the acrylic plate, q_{sus} the corrected heat flux in the stainless steel foil, and q_{rad} the radiative heat flux. The positive and negative values in each heat flux (q_{aor} and q_{sus}) mean "inflow" to a pixel and "outflow" from a pixel, respectively.

Experimental Uncertainties

All the uncertainties were estimated by the procedure described by ANSI/ASME, PTC 19-1 (1985) and Moffat (1988). The main sources of errors in Nusselt number were the evaluation of the temperature, the heat flux, the thermal conductivity of the fluid, and the size of nozzle diameter. Their bias limits were representatively 0.11°C for *Tw* from 35 to 42°C, 0.84 W/m² for q_{net} = 206 W/m², 4.55×10^{-6} W/(m·K) for λ = 0.023 W/(m·K) and 0.05 mm for D = 30 mm. Their precision limits were 0.018°C, 0.12 W/m², 1.28×10^{-7} W/(m·K) and 0 mm, respectively. The partial derivatives of the Nusselt number with respect to the variables were determined numerically using finite difference method. Consequently, a 95 percent relative coverage of uncertainty for Nusselt number was from 1.62 to 6.01 percent depending on flow condition. On the other hand, a 95 percent relative coverage of uncertainty for flow velocity was 5.1 percent.

Experimental Results and Discussions

Impingement Surface Temperature. Figures 3(*a, b, c*) and 4(*a, b, c*) show the temperature visualization and the isothermal distribution for various inclination angles (θ = 90, 60, and 45 deg) for Re = 2 × 10⁴, respectively. The abscissa is dimensionless distance X and the ordinate is the dimensionless distance Y. The origin (0, 0) is the geometric center, which means that a line extending from the nozzle center intersects the impingement surface. Image smoothing was used twice before the contour print was made. In the case of θ = 90 deg (Fig. 3*a*), the jet is normal

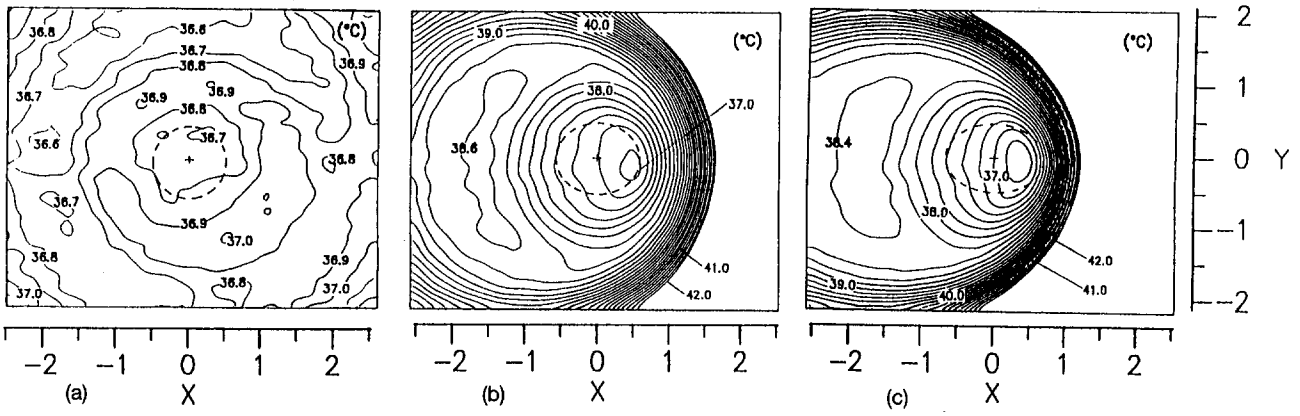

Fig. 4 Isothermal line (Re = 2 × 10⁴): (a) θ = 90 deg, (b) θ = 60 deg, (c) θ = 45 deg

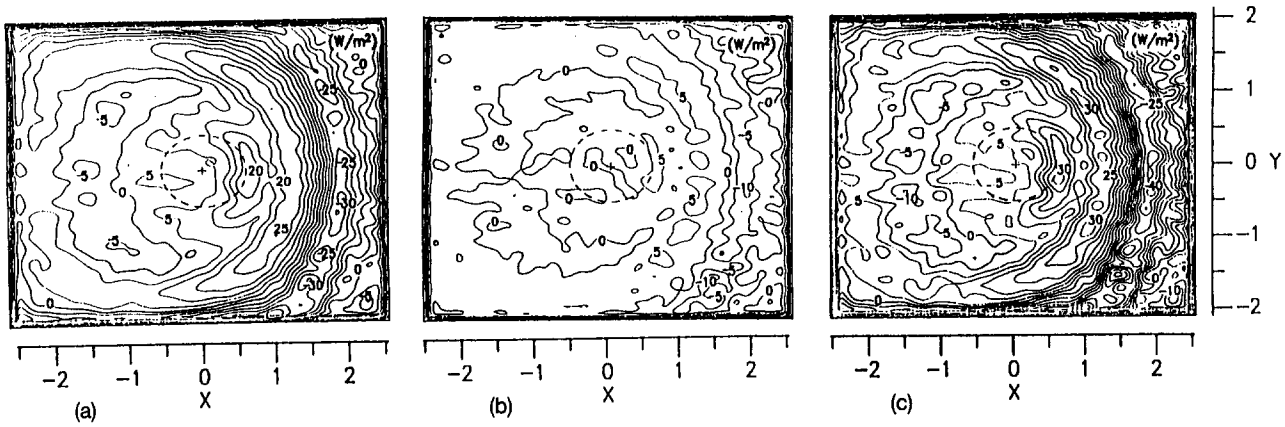

Fig. 5 Corrected heat flux (Re = 2×10^4, θ = 60 deg): (*a*) q_{acr}, (*b*) q_{sus}, (*c*) q_{cond}

to the impingement surface and a yellow and light blue annular pattern is shown on the impingement surface. The radius of the annular region ranges from dimensionless length 1 to 1.5. For θ = 60 deg (Fig. 3*b*), the high-temperature region moves to the downflow side of the low-temperature region (color: light brown) where the jet impinged directly. The distribution is symmetric for $Y = 0$ and is shaped like a horseshoe type. This tendency becomes marked for θ = 45 deg (Fig. 3*c*). That temperature step in Fig. 4 is 0.1 ~ 0.2°C. The dotted line shows the region at which the extension of the nozzle end intersected with the impingement surface. The inner circle of the annular temperature distribution moves to the right-hand side where the temperature gradient becomes high. Concretely, for θ = 60 deg (Fig. 4*b*) the temperature increase is about 5°C from $X \fallingdotseq 0.5$ to $X \fallingdotseq 1.6$ and on the other hand, it is about 1.6°C from $X \fallingdotseq 0.5$ to $X \fallingdotseq -1$. A plateau section appears from $X \fallingdotseq -1$ to $X \fallingdotseq -2$ for θ = 60 deg and from $X \fallingdotseq -1.2$ to $X \fallingdotseq -3$ for θ = 45 deg (Fig. 4*c*) at Re = 2×10^4. The plateau section appears generally at comparatively high Reynolds number (more than Re = 5000) and extends in the Y direction with increase of Reynolds number. For θ = 45 deg, isothermal lines also extend to the negative region of X because the ellipticity of the nozzle end becomes larger.

Corrected Heat Flux. The heat flow in the heated section was evaluated by using the detailed temperature distribution. Figures 5(*a, b, c*) show the corrected heat fluxes in the acrylic plate, the stainless steel foil, and the total corrected heat flux with heat flux step 5 W/m^2 for θ = 60 deg and Re = 2×10^4. The positive value means "inflow" and the negative value, "outflow." The lines 0 W/m^2 in q_{acr} exist in the shape of a horseshoe near X = +2.0 and $X = -0.5 \sim -2.0$. The heat of comparatively high absolute value (from +25 to −30 W/m^2) flows in or out at the positive side from the geometric center and on the other hand, the heat of lower absolute value (from −5 to +5 W/m^2) flows in or out at the negative side. Heat flows from the outside to the inside of the horseshoe region. In the stainless steel foil, the heat flow q_{sus} is qualitatively the same as q_{acr} in the acrylic plate. However, the absolute value is of a lower level. Consequently, the total corrected heat flux q_{cond} has comparatively higher values at the positive side and lower values at the negative side. The ratios of the corrected heat flux in the heated section and the uniform heat flux by Joule heating, q_{cond}/q_{unif}, are +16.9 ~ −14.5 percent at Re = 2000, +12.7 ~ −10.6 percent at Re = 10,000 and +6.4 ~ −8.5 percent at Re = 2×10^4. The effect of thermal radiation is from 1 to 2.9 percent. The heat flow in the impingement section has not been considered precisely in previous studies.

Local Heat Transfer. Local Nusselt numbers are represented in Figs. 6(*a, b, c*) corresponding to Figs. 3 and 4. In the case of θ = 90 deg (Fig. 6*a*), the local Nusselt number assumes a peak near the stagnation point for laminar jet and two peaks (radius from the center $X \fallingdotseq 0.5$ and 1.5) in annular form for turbulent jet (Ichimiya and Nakamura, 1992). Local distribution is not symmetric because the perfect symmetric flow was not realized in practice and the space resolution of the present measurement was better than that of previous methods. In the case of θ = 60 deg (Fig. 6*b*), the peak changes to the right edge of the dashed ellipse and a plateau section exists in the major flow region (the negative direction of X). This section extends in the negative direction of X with the decrease of the inclination angle and in the case of turbulent jet. This tendency is different from the behavior of the iso-Nusselt number that Goldstein and Franchett (1988) obtained. This depends on the confined walls and the

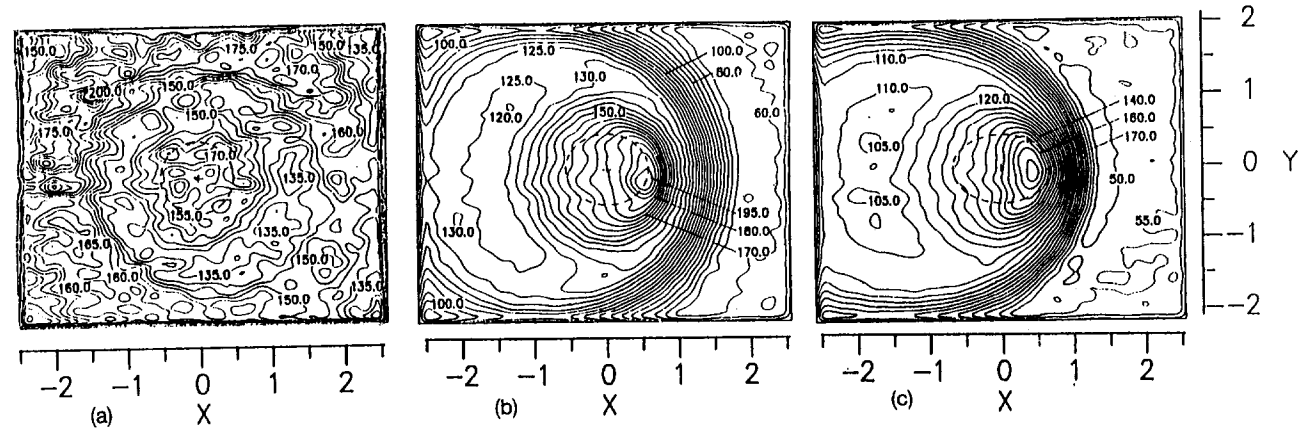

Fig. 6 Local Nusselt number (Re = 2×10^4): (*a*) θ = 90 deg, (*b*) θ = 60 deg, (*c*) θ = 45 deg

space resolution of temperature measurement. In the case of θ = 45 deg (Fig. 6*c*), the Nusselt number gradient becomes steeper and the position of the peak moves to the inside of the dashed ellipse. Figures 7(*a, b, c*) show the topography contours, which represent the entire behavior of the local Nusselt numbers. According to the figures, the local irregular distribution for θ = 90 deg is flattened by inclined jets (θ = 60 and 45 deg). Figures 8(*a, b, c*) show the local Nusselt numbers along the center line of the impingement surface with and without the correction of the local heat flux for Re = 2000 and 2×10^4. The solid line denotes the local Nusselt number for the net heat flux q_{net} and the dashed line that for the uniform heat flux q_{unif}. The net heat flux improves the maximum and minimum of local Nusselt numbers. This effect is especially noticeable at low Reynolds numbers, which appears to justify the examination of local Nusselt number in detail by considering the correction of local heat flux.

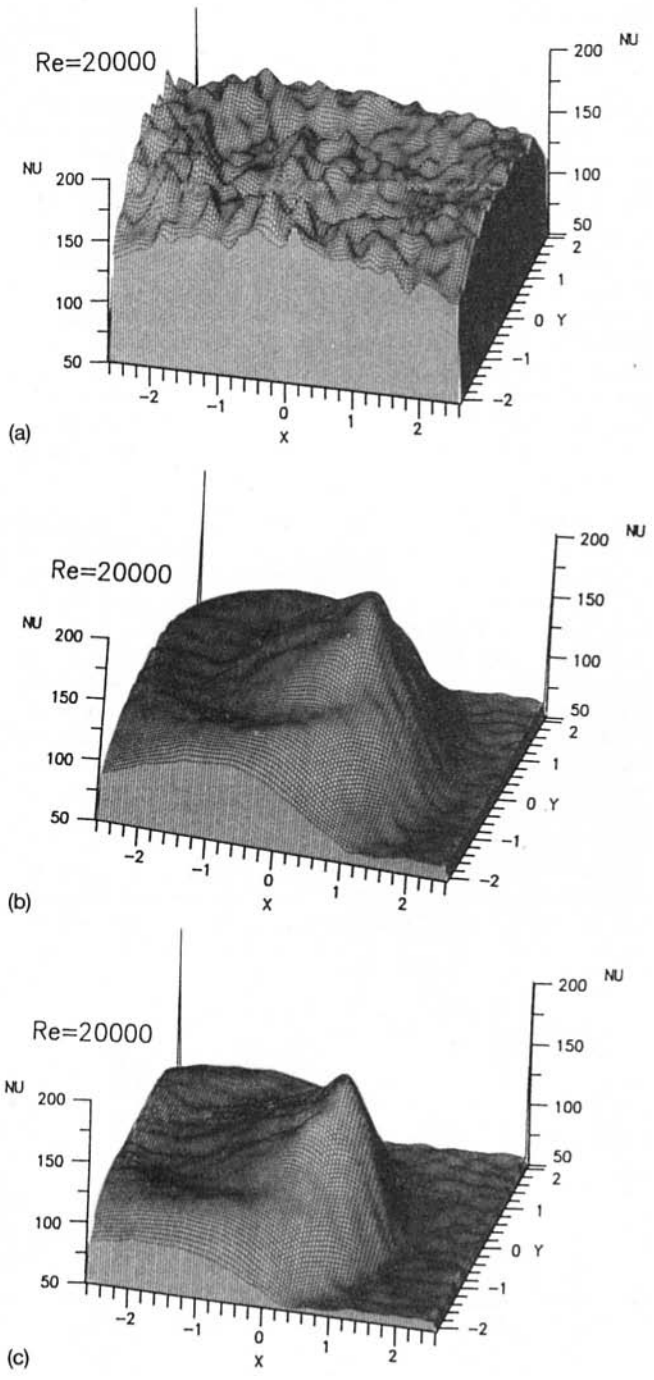

Fig. 7 Topography contours of local Nusselt number (Re = 2×10^4): (*a*) θ = 90 deg, (*b*) θ = 60 deg, (*c*) θ = 45 deg

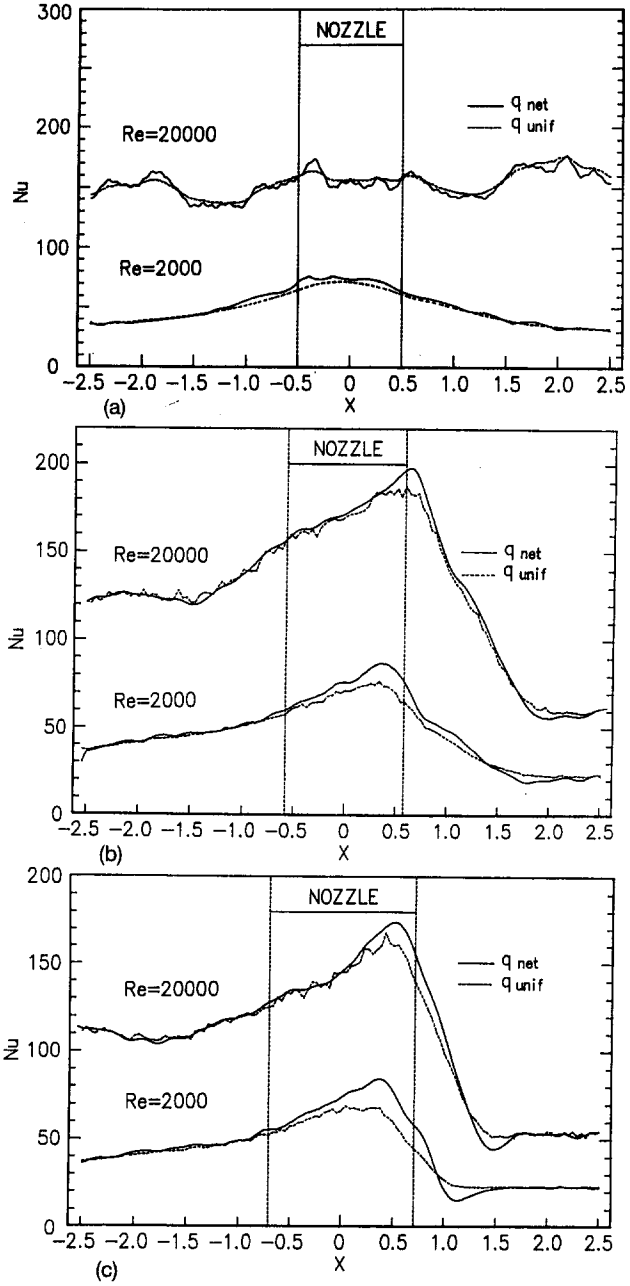

Fig. 8 Effect of heat flux correction on Nusselt number: (*a*) θ = 90 deg, (*b*) θ = 60 deg, (*c*) θ = 45 deg

Flow Field. The flow was measured and found to be related to the local heat transfer. Figures 9(*a, b*) represent the dimensionless velocity and the turbulent intensity for θ = 60 deg and Re = 2×10^4, respectively. The dimensionless value is obtained in terms of the maximum velocity at the nozzle exit (U_{max} = 13 m/s). The symbol ∇ and $X = 0$ denote the center of nozzle and the geometric center, respectively. The jet from the nozzle crossed through the surrounding stationary fluid and impinged on the flat surface. The actual stagnation point existed between the geometric center and the nozzle edge. The rolling back of the flow (vortex) and the amplification of turbulence near the impingement surface in the region of the minor flow ($0 \leq X \leq 0.5$) peaked the local heat transfer, as noted in Fig. 8. Although the flow is decelerated from $X \fallingdotseq -1$ to $X \fallingdotseq -2.5$ at the major flow region and the absolute value of the turbulence intensity is com-

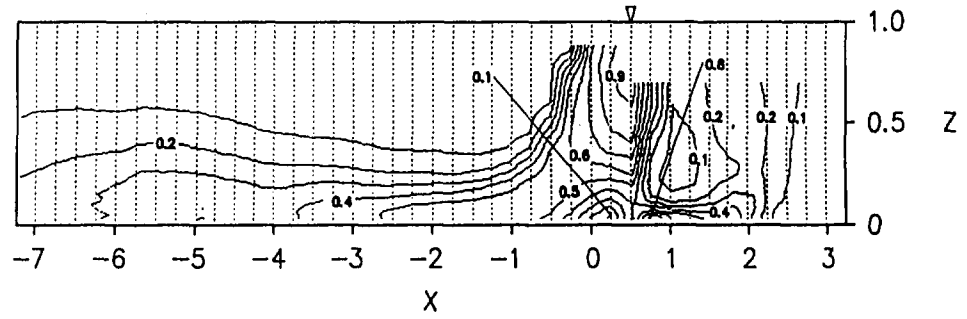

(a) Dimensionless velocity u/u_{max}

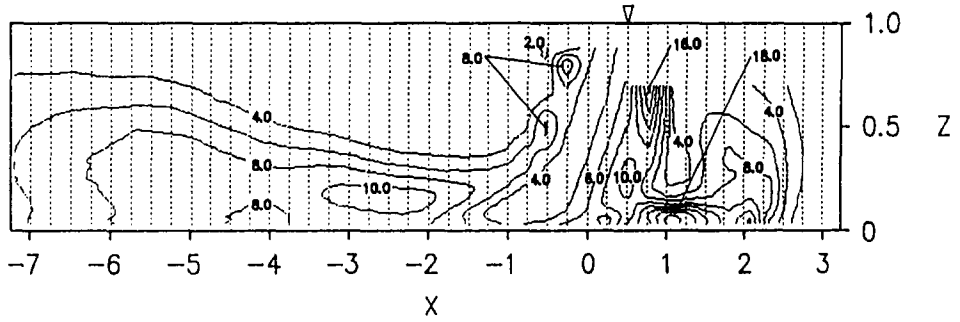

(b) Turbulence intensity $\sqrt{u'^2}/u_{max} \times 100$ percent

Fig. 9 Flow field (Re = 2×10^4, θ = 60 deg; Y = 0)

paratively high, the gradient is mild. As a result, the heat transfer improvement at the major flow region is not as significant as that at the minor flow region. The gradients of these physical parameters seem to affect the local heat transfer augmentation as their absolute values do. The power spectrum of the velocity fluctuation at $X = -1$, $Y = 0$, $Z = 0.017$ for $\theta = 60$ deg and Re = 2×10^4 is presented in Fig. 10. The superior frequency (the spike in the power spectrum) that causes the local heat transfer augmentation is from 150 Hz to 250 Hz for Re = 2×10^4 and 150 Hz for Re = 10^4, and consequently this depends on Reynolds number. These frequencies were also the same as those for $\theta = 45$ deg. However, in the present stage, it is not clear why this superior frequency affects heat transfer augmentation. These correlations should be examined in detail in the future.

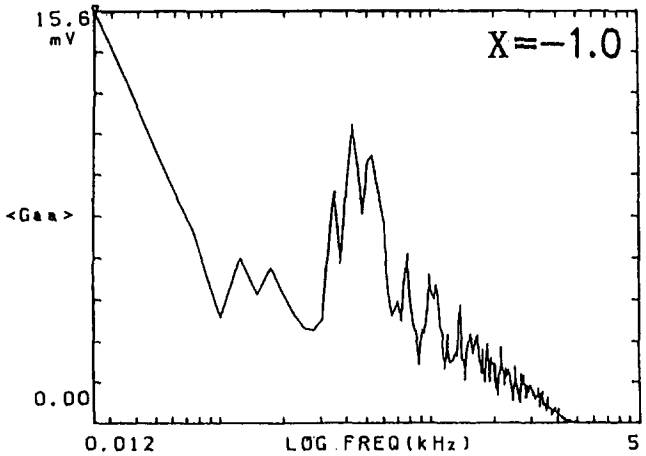

Fig. 10 Power spectrum (Re = 2×10^4, θ = 60 deg, $X = -1.0$, $Y = 0$, $Z = 0.017$)

Conclusions

The heat transfer and flow characteristics of an oblique circular air jet with confined walls were investigated experimentally at $h/D = 1.0$ for θ = 90, 60, and 45 deg. The local temperature on the impingement surface was obtained in detail by a thermocamera using a liquid crystal sheet.

1 The local Nusselt number showed the characteristic peak shift in the minor flow region and the plateau in the major flow region. The local turbulent intensity and the acceleration near the impingement surface depending on the inclination angle and the Reynolds number corresponded to the behavior of the local heat transfer.
2 The effect of the correction of the local heat flux in the heated section is marked at low Reynolds number and amounts to about 6 ~ 17 percent of uniform heat flux.
3 Vortex generation and amplification of turbulence in the minor flow region cause the local heat transfer increase.
4 The superior frequency in power spectrum of velocity fluctuation affecting heat transfer enhancement ranges from 150 to 250 Hz and depends on Re within the present conditions.

Acknowledgments

The author wishes to acknowledge the financial support by the Ministry of Education from the research project grant-in-aid for scientific research (c) and thanks to Mr. T. Nasu, Mitsubishi Heavy Industries Co. Ltd., who assisted the experiment.

References

Akino, N., Kunugi, T., Ichimiya, K., Mitsushiro, K., and Ueda, M., 1989, "Improved Liquid-Crystal Thermometry Excluding Human Color Sensation," ASME JOURNAL OF HEAT TRANSFER, Vol. 111, pp. 558–565.

ANSI/ASME PTC 19-1, 1985, "Supplement to Performance Test Coded, Instrument and Apparatus. Part 1—Measurement Uncertainty," ASME, New York.

Foss, J. F., and Kleis, S. J., 1976, "Mean Flow Characteristics for the Oblique Impingement of an Axisymmetric Jet," *AIAA Journal,* Vol. 14, No. 6, pp. 705–706.

Foss, J. F., 1979, "Measurement in a Large-Angle Oblique Jet Impingement Flow," *AIAA Journal,* Vol. 17, No. 8, pp. 801–802.

Goldstein, R. J., and Franchett, M. E., 1988, "Heat Transfer From a Flat Surface to an Oblique Impinging Jet," ASME JOURNAL OF HEAT TRANSFER, Vol. 110, pp. 84–90.

Han, L. S., Kayansayan, N., and Dantzer, C. W., 1983, "Impingement Cooling of Turbine Airfoils by Multiple Two-Dimensional Jets," *Proc. Tokyo International Gas Turbine Congress,* pp. 75–82.

Hollworth, B. R., and Durbin, M., 1992, "Impingement Cooling of Electronics," ASME JOURNAL OF HEAT TRANSFER, Vol. 114, pp. 607–613.

Ichimiya, K., Kobayashi, K., and Echigo, R., 1987, "Basic Study on the Flattening of Temperature Distribution of Steel Slab for Direct Rolling (Unsteady-State Heat Transfer in Heat Conductive-Convective Field on the Flattening of Temperature Distribution)," *Proceedings of 2nd ASME/JSME Thermal Engineering Joint Conference,* Vol. 5, pp. 79–84.

Ichimiya, K., and Nakamura, Y., 1992, "Heat Transfer of a Single Circular Impinging Jet Considered on Heat Conduction in a Heated Plate," *Transactions of JSME(B),* Vol. 58, No. 550, pp. 2031–2035.

Jambunathan, K., Lai, E., Moss, M. A., and Button, B. L., 1992, "A Review of Heat Transfer Data for Single Circular Jet Impingement," *International Journal of Heat and Fluid Flow,* Vol. 13, No. 2, pp. 106–115.

Kamoi, A., and Tanaka, H., 1977, "Study on Two-Dimensional Impingement Jet Flow Considered Initial Turbulence (Part 2, Static Characteristics of Boundary Layer in Stagnation Region)," *Transactions of JSME,* Vol. 43, No. 372, pp. 2957–2969.

Kunugi, T., Akino, N., Ichimiya, K., and Takagi, I., 1991, "Evaluation of Heat Conduction and Visualization of Heat Flux in a Plate Making Use of Heat Transfer Experiments," *Experimental Thermal and Fluid Science,* Vol. 4, pp. 448–451.

Martin, H., 1977, "Heat and Mass Transfer Between Impinging Gas Jets and Solid Surface," *Advances in Heat Transfer,* Vol. 13, Academic Press, New York, pp. 1–60.

McMurray, D. C., Myers, P. S., and Uyehara, O. A., 1966, "Influence of Impingement Jet Variables on Local Heat Transfer Coefficients Along a Flat Surface With Constant Heat Flux," *Proceedings of 3rd International Heat Transfer Conference,* Vol. 2, pp. 292–299.

Moffat, R. J., 1988, "Describing the Uncertainties in Experimental Results," *Experimental Thermal and Fluid Science,* Vol. 1, pp. 3–17.

Rubel, A., 1981, "Computations of the Oblique Impingement of Round Jets Upon a Plane Wall," *AIAA Journal,* Vol. 19, No. 7, pp. 863–871.

Rubel, A., 1982, "Oblique Impingement of a Round Jet on a Plane Surface," *AIAA Journal,* Vol. 20, No. 12, pp. 1756–1758.

Sparrow, E. M., and Lovell, B. J., 1980, "Heat Transfer Characteristics of an Obliquely Impinging Circular Jet," ASME JOURNAL OF HEAT TRANSFER, Vol. 102, pp. 202–209.

Stevens, J., and Webb, B. W., 1991, "The Effect of Inclination on Local Heat Transfer Under an Axisymmetric, Free Liquid Jet," *International Journal of Heat and Mass Transfer,* Vol. 34, pp. 1227–1236.

Viskanta, R., 1993, "Heat Transfer to Impinging Isothermal Gas and Flame Jets," *Experimental Thermal and Fluid Science,* Vol. 6, No. 2, pp. 111–134.

Ward, J., Oladiran, M. T., and Hammond, G. P., 1991, "The Effect of Nozzle Inclination on Jet-Impingement Heat Transfer in a Confined Cross-Flow," *Fundamentals of Forced Convective Heat Transfer,* ASME HTD-Vol. 181, pp. 25–31.